BNL--37358
DE86 006246

PROGRESS IN SEMICONDUCTOR DRIFT DETECTORS

Pavel Rehak
Brookhaven National Laboratory, Upton, NY 11973, USA

Jack Walton
Lawrence Berkeley Laboratory, Berkeley, CA 94720, USA

Emilio Gatti, Antonio Longoni and Marco Sanpietro
Dipartimento di Elettronica,
Politecnico di Milano, Piazza Leonardo da Vinci, 32,
20133 Milano, Italy

Josef Kemmer
Fakultät für Physik der Technischen Universitat München, FRG

Hans Dietl, Peter Holl, Robert Klanner, Gerhard Lutz and Andrew Wylie
Max Planck Institut für Physik und Astrophysik, München, FRG

Hubert Becker
Fachhochschule Saarbruecken, FRG

Invited Talk presented at the
IEEE 1985 Nuclear Science Symposium 10/23-25
Sheraton-Palace Hotel, San Francisco, CA

PROGRESS IN SEMICONDUCTOR DRIFT DETECTORS*

Pavel Rehak
Brookhaven National Laboratory, Upton, NY 11973, USA

Jack Walton
Lawrence Berkeley Laboratory, Berkeley, CA 94720, USA

Emilio Gatti, Antonio Longoni and Marco Sanpietro
Dipartimento di Elettronica, Politecnico di Milano, Piazza Leonardo da Vinci, 32, 20133 Milano, Italy

Josef Kemmer
Fakultät für Physik der Technischen Universitat München, FRG

Hans Dietl, Peter Holl, Robert Klanner, Gerhard Lutz and Andrew Wylie
Max Planck Institut für Physik und Astrophysik, München, FRG

Hubert Becker
Fachhochschule Saarbruecken, FRG

Abstract

Progress in testing semiconductor drift detectors is reported. Generally better position and energy resolutions were obtained than resolutions published previously. The improvement is mostly due to new electronics better matched to different detectors. It is shown that semiconductor drift detectors are becoming versatile and reliable detectors for position and energy measurements.

1. Introduction

Semiconductor drift detectors were recently proposed [1,2]. The first detector working on this new idea was produced at LBL in 1983 [3]. At the beginning of 1984 several drift detectors were produced at TU-München. A description of these detectors, along with an account of their production and first results of their performances, is published in Ref. [4].

In this paper we report new test results of detectors produced at TU-München. We compare their actual performance with the performance derived from the theory of these detectors. We point out shortcomings of the existing detectors and discuss possible improvements. To keep this paper short we will often refer to published articles. Section 2 describes briefly the principles of semiconductor drift detectors. Section 3 which deals with the position measurement in silicon drift detectors is divided into two parts. Part A describes results obtained from tests of a continuous anode detector; Part B deals with the test of a multi-anode chamber. Section 4 is dedicated to the energy measurement with drift detectors. Parts A and B describe results of tests at room temperature and liquid nitrogen temperature, respectively. Part C deals with practical biasing of detectors and Part D describes a method of self timing. We will conclude with a list summarizing the achieved performance of silicon drift detectors.

2. Principles of Semiconductor Drift Detectors

Fig. 1 shows the principle of semiconductor drift detectors [1,2]. The novel feature of this relatively new detector is a transport of electrons

*Research partially supported by the US Department of Energy, contract No. DE-AC02-76CH00016, by the Italian INFN, MPI and CNR and by the Bundesministerium für Forschung und Technologue, W. Germany.

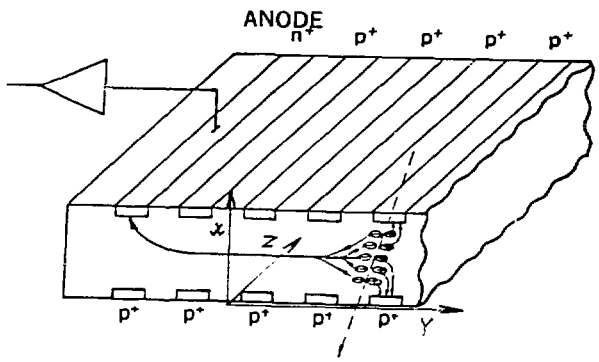

Fig. 1.

parallel to large surfaces of the detector onto a small area anode (n^+ electrode) connected to the input of an amplifier. The controlled transport of electrons, created by a detected particle, from point of origin to the anode has the two following advantages.

i) The drift time of electrons within the detector depends on the electron drift distance. The drift detector is thus a position sensitive detector.

ii) The capacitance of the anode is small and practically independent of the detector size. The small anode capacitance decreases the effect of the preamplifier series noise. Low noise detection systems with large detectors are possible to realize with the new detector.

The electric field responsible for the electron transport inside the detector of Fig. 1 is shown in Fig. 2. The potential energy of electrons (or negative electric potential) is shown in the x,y plane. The potential does not depend on the z-coordinate along the rectifying p^+n junction; the potential problem is thus two dimensional. The detector made from n-type silicon is fully depleted of free carriers, hence the negative potential has to satisfy Poisson's equation:

$$\frac{\partial^2(-\phi)}{\partial^2 x} + \frac{\partial^2(-\phi)}{\partial^2 y} = \frac{N_D \cdot q}{\varepsilon_0 \varepsilon_r} \qquad (1)$$

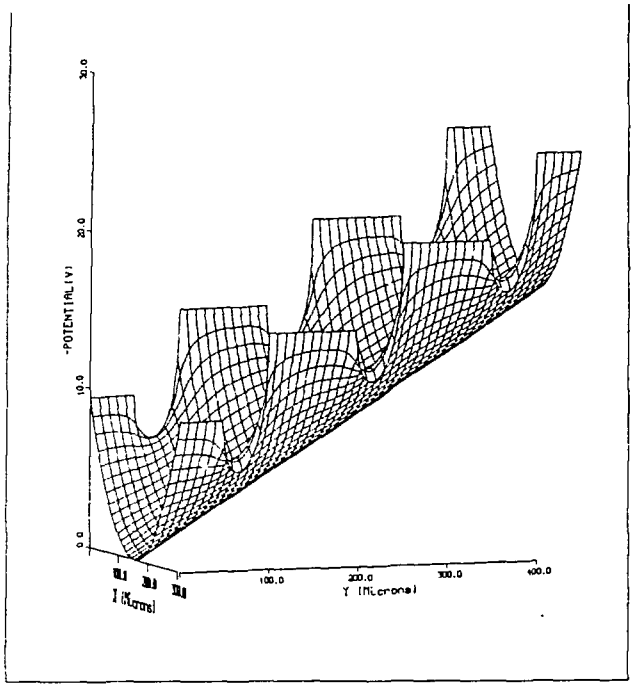

Fig. 2.

where N_D is the density of ionized donors in silicon bulk; ε_r is the relative dielectric constant; q and ε_0 have their usual meaning of electronic charge (positive) and permeability, respectively. The potential shown in Fig. 2 is a close realization of an ideal Φ_i potential (shown in Fig. 2 of Ref. [3]) which is a sum of a linear potential along the y-coordinate (drift coordinate) and a parabolic potential along the x-coordinate.

$$-\Phi_i(x,y) = \frac{N_D \cdot q}{2\varepsilon_0\varepsilon_r} \cdot (x-x_0)^2 + E_D \cdot y \qquad (2)$$

where x_0 is the x-coordinate of the minimum of the electron potential energy and E_D is the drift field. The potential of Fig. 2 was realized by applying appropriate voltages to the linear array of rectifying p^+v junctions. The detector surface between two adjacent junctions is covered by thermally grown SiO_2. Positive charges in the oxide define the remaining boundary conditions on $Si-SiO_2$ interface.

Electrons created by fast particles crossing the detector are focused by the field into the center plane of the detector and transported in this plane towards the anode. The drift time of electrons is measured as the delay of signal induced on the anode by a cloud of arriving electrons relative to the crossing time of the fast particle. The electron drift time is proportional to the distance between anode and the place where electrons were created by the passage of a fast particle.

The electric field has a different shape in the region of the detector close to the anode. Here the minimum of the electron potential energy is shifted from the central plane of the detector toward the anode side of the detector. The potential of this anode region is shown in Fig. 4 of Ref. [3]. More information about drift detectors and their production can be found in Refs. [4] and [5].

3. Position Measurements with Silicon Drift Detectors

A detailed analysis of position measurement in silicon drift detectors was presented in Ref. [3]. The shape of a filter which optimizes the position resolution was derived. The filter takes into account

i) electron diffusion (and mutual repulsion of electrons) during the drift to the anode;
ii) series noise of the preampliier, and;
iii) detector leakage current.

The electron diffusion is rather large due to a relatively long drift time of electrons ($\sigma \approx 100$ μm for practical distances and practical values of the drift field E_D). The optimum filtering essentially finds the centroid of drift times for all electrons arriving at the anode and keeps the fluctuations from the remaining noise sources small. The predicted position resolution is about 4 μm for a drift distance of 4 mm.

A. Continuous Anode Detector

The silicon detector on which tests were performed is shown in Figs. 2 and 3 of Ref. [4]. The length of the anode is 10mm and maximum drift distance is 4 mm. As described in Ref. [4] two anodes are used to remove the right-left ambiguity.

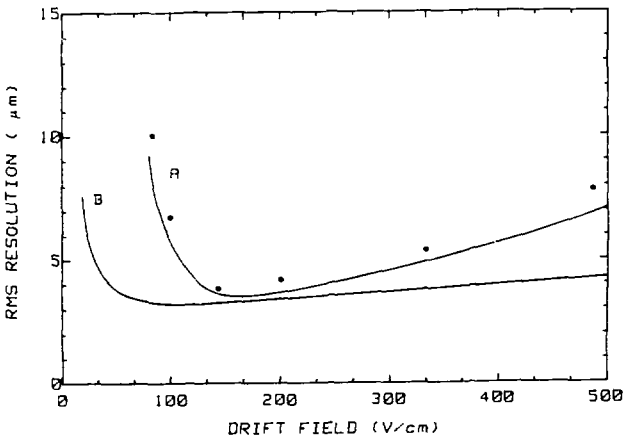

Fig. 3

Figure 3 shows the resolution as a function of drift field E_D for a constant drift distance d = 3.85 mm. Experimental points are shown by black dots. Curve A shows the calculated resolution for filter used in the measurement and optimized for a drift field E_D = 150V/cm. Curve B shows the best resolution obtainable if optimized filters were used for all values of the field E_D. The resolution shown in Fig. 3 was obtained under laboratory conditions with light pulses focused on the surface of the detector. The light intensity was adjusted to produce the same number of electrons as a minimum ionizing particle passing through the detector. The r.m.s. of the distribution of drift time for light pulses was measured for each value of E_D and multiplied by the drift velocity to obtain the position resolution.

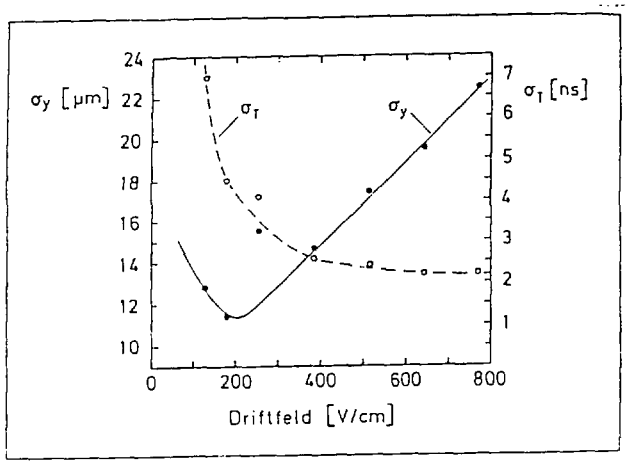

Fig. 4

Figure 4 shows the resolution of the same detector obtained with minimum ionizing particles [6]. The test was performed at the CERN SPS with the help of equipment of the NA32 experiment. The position of 100 GeV/c π^- was measured in the NA32 silicon microstrip detectors and the position of π^- predicted in the plane of the drift detector. The distribution of the differences between the predicted position and measured position in the drift detector was produced for each value of the drift field E_D. The error in the predicted position from the microstrip detectors ($\approx$ 7 μm) was subtracted in quadrature from the r.m.s. of total differences and plotted in Fig. 4 as a function of the drift field. The best resolution obtained in the beam test is about 11 μm for a drift field of 200V/cm.

Let us list the possible reasons for the deterioration of the resolution in the beam test and suggest ways to achieve its "theoretical" value.

a) Temperature dependence of the electron mobility μ. For pure n-type silicon near room temperature the electron mobility varies as $T^{-2.42}$[7] (T is the absolute temperature). To keep the electron mobility constant within one part in thousand the temperature has to be constant within 0.13°C.

The temperature remains sufficiently constant during lab measurements with the light pulser, where one measurement lasts typically only a few minutes. This may not be the case for the beam test where a measurement at one value of the drift field lasts several hours.

To control the temperature of silicon detectors within 0.13°C might not be practical in a real experiment. Continuous calibration by injecting a charge into a given position in the detector at a given time would track the changes in the electron mobility and remove the error due to temperature changes.

b) Differential nonlinearities. For the ideal potential $\phi_i(x,y)$ given by Eq. (2), the electron drift time is strictly proportional to the drift distance in the y direction independently of the x-coordinate. In a drift detector with a potential as shown in Fig. 2 there is a slight dependence of the electron drift time on the x-coordinate of the origin of the ionization. Fig. 5 shows the calculated dependence of the mean drift time of electrons produced

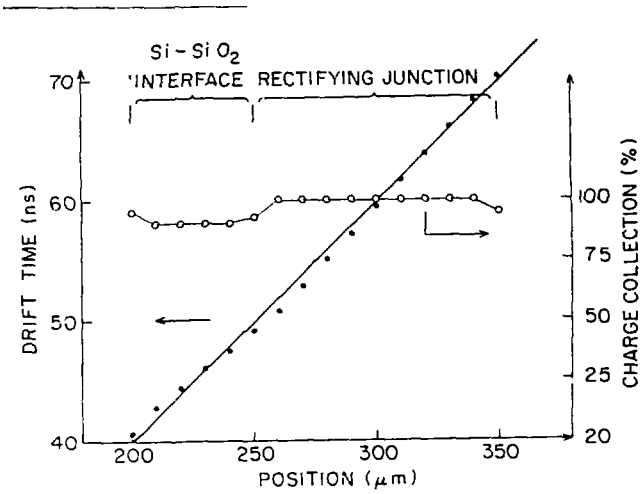

Fig. 5

uniformly across the thickness of the detector (y=const.) on the drift coordinate y. One pitch of the drift structure, that is, the sum of the width of the rectifying junction and the width of $Si-SiO_2$ interface is shown. (Position coordinate in Figs. 5 and 6 corresponds to the y-coordinate of Fig. 2.)

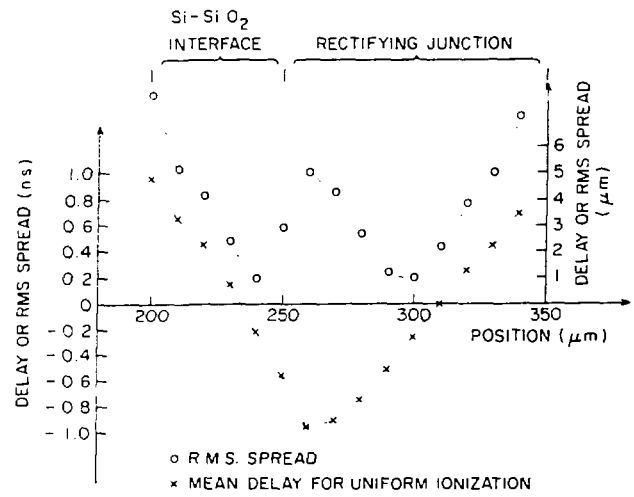

Fig. 6

Crosses on Fig. 6 show deviation from the linear dependence in ns (left scale) and μm (right scale). The effect of differential nonlinearity was observed in the beam test and is shown in Fig. 18 of Ref. [4]. The nonlinearity can be corrected by a nonlinear drift distance-drift time calibration on-line or off-line. It is also not difficult to produce and to operate a drift detector with the drift structure pitch of less than 75 μm. In such a fine structure the effect of differential nonlinearity should be negligible. Closely related to the differential nonlinearity is:

c) Nonideal isochronism. Electrons created at the same y-coordinate but at different depth x within the detectors reach the anode at slightly different times. The r.m.s. of this spread for uniform ionization across the detector is also plotted in Fig. 6. Fluctuations in the density of the ionization along the path of the particle produce fluctuations in the drift time measured as the arrival of the centroid of the total charge.

Let us estimate the effect of the nonideal isochronism for the "Landau" fluctuations of the ionization density of minimum ionizing particles. The statistical ensemble consists of particles with fluctuating density of ionization crossing the detector at a given coordinate y. We have to calculate the ensemble variance of the arrival time of the centroid of the charge of electrons produced by the ionization.

The arrival time of a single event of the ensemble is defined as:

$$t = \int_0^d t(x)\cdot q(x)dx \Big/ \int_0^d q(x)dx \doteq \sum_j^N t(x_j)\frac{q(x_j)\Delta x}{\sum_i q(x_i)\Delta x}$$

$$= \sum_j^N t(x_j)\cdot W_j(x_1,x_2\ldots x_N) \qquad (3)$$

where $t(x)$ denotes the drift time of an electron created at the depth x inside the detector, d is the detector thickness, $q(x)$ the ionization density at x, and W_j the statistical weight. For our calculation it is convenient to approximate the integral by a sum of N small intervals Δx covering the detector thickness. We notice that $W_j(x_1,x_2\ldots x_N)$ depends on the ionization in all intervals Δx. The variance of t is a double sum

$$\mathrm{var}(t) = \sum_{j,i} t(x_j)t(x_i)\cdot\mathrm{cor}(W_j,W_i) \qquad (4)$$

We simplify the calculation by the assumption of zero correlation between ionization densities at different coordinates x. Correlations between statistical weights W-s can be then calculated by a standard method of Taylor's expansion around their mean values.

$$\mathrm{cor}(W_j,W_i) = \frac{\mathrm{var}(q)}{N^3\,\bar{q}^2}\left(N\delta_{j,i}-1\right) \qquad (5)$$

where var(q) is the variance of density q (independent of interval number), q is the mean density and δ_{ji} has its usual meaning as the Kronecker symbol. Substitution of (5) into (4) gives after some elementary manipulations.

$$\mathrm{var}(t) = \frac{\mathrm{var}Q}{\bar{Q}^2}\cdot(\delta t)^2 \qquad (6)$$

or

$$\sigma_t = \frac{\sigma_Q}{\bar{Q}}\cdot\delta t;\quad \sigma_\ell = \frac{\sigma_Q}{\bar{Q}}\cdot\delta\ell \qquad (7)$$

where δt (or $\delta\ell$) is the r.m.s. of the time (or position) spread as plotted in Fig. 6; $\bar{Q} = N\cdot q\cdot\Delta x$ is the mean value of the total ionization and var(Q) is its variance. The relative width $\sigma_Q/\bar{Q}$ of the Landau distribution is experimentally known (Fig. 17 of Ref. 4) to be about 20%. Taking the experimental value of the relative width of the ionization fluctuation in the detector we correct to some extent the error made by our assumption of zero correlation between densities of ionization at different depth of the detector.

Equation 7 gives for our detector $\sigma_t \doteq .4$ns or $\sigma_\ell \doteq 2$ μm. Equation 7 may be too optimistic. If the real error is twice the error predicted by Eq. 7 the lack of perfect isochronism contributes significantly to the deterioration of the detector position resolution for the minimum ionizing particles.

These fluctuations cannot be corrected by any sophisticated calibration for the existing drift detector. To decrease the effect to a negligible level a drift detector with a finer structure of drift electrodes has to be produced.

d) Misalignment of drift electrodes on two sides of the detector. Due to an error in the mask design drift electrodes on one side of the detector are shifted by 20 μm relative to the other side. The misalignment is equivalent to a nonperpendicular incident angle of particles to the surface of the detector. Electrons produced by the ionization along the particle path reach the anode at different times. Previous analysis of deviations from isochronism is directly applicable to our misalignment and also generally applicable for an evaluation of the position resolution for particles incident on the detector at any angle.

Eq. 7 for $\delta\ell = 20\mu m/\sqrt{12} = 7\mu m$ gives $\sigma_\ell = 2$ μm.

e) Electronic noise of the second amplifier stage. The stability of the shaping amplifiers used simultaneously in the beam test required the termination of cables at their input. The termination lowered the effective gain of the preamplifier by a factor of 2 and the noise of the second stage contributed to the deterioration of the resolution. Presently we have a new electronics system which eliminates the problem.

To close the list of possible reasons for the difference between the position resolution obtained in the lab and in the beam, we would like to stress that the relative resolution already achieved in the beam test corresponds to an impressive ratio of 1 in 400.

B. Position Resolution of Multi-anode Detector

Figure 6 in Ref. [5] shows the multianode drift detector. The single line anode of Fig. 1 has been segmented in 41 square pad anodes. Each pad anode is read out by different preamplifiers followed by a complete chain of electronics. Drift time and total charge is measured for each anode. Drift time measures the y-coordinate as in the previous case of a continuous anode; division of charge among individual anodes measures the z-coordinates. (The charge sharing among anodes is due to the diffusion and mutual repulsion of electrons during their drift within the detector.) Multianode chambers thus measure both coordinates of particles in an unambiguous way. A natural consequence of a larger number of readout channels is an increase of the number of particles which can be measured within the detector for the same interaction event.

Figures 7 and 8 show results of a preliminary test of the multianode detector. Tests were performed at the CERN SPS in a similar way as the beam test of a continuous anode detector. Figures 7

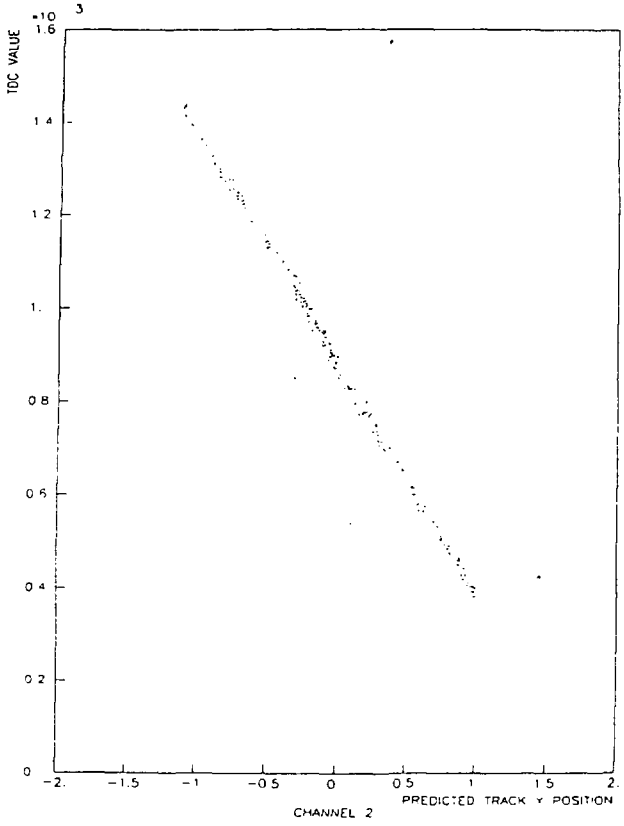

Fig. 7

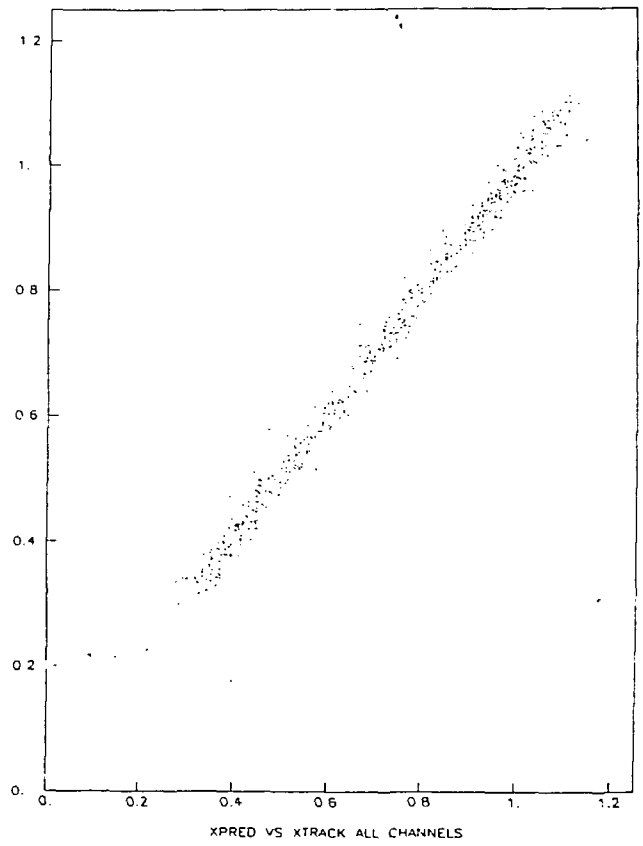

Fig. 8

and 8 show the scatter plot of the position measured in the multianode detector versus position predicted from strip detectors in the y-(drift) coordinate and z-coordinate, respectively.

The measured resolution is about 18 μm and 24 μm. From Fig. 8 one can deduce a root mean square of residuals (predicted minus measured position) of 31 μm. The r.m.s. of the prediction is 20 μm which leads to above mentioned value of 24 μm.

There is a visible kink on the scatter plot of Fig. 7. We believe it is due to the distortion in the predicted position from strip detectors which were damaged by beam radiation. We were not aware of the damage and of the distortion of strip detectors during the test.

For all the reasons discussed in the previous part plus additional difficulties with the prediction of the position from the measurement in the strip detectors the measured resolution can be considered only as an upper limit The calculated resolution along the drift coordinate is shown in Fig. 9 for 3 different filters as a function of the drift distance.

Before discussing the energy measurements in the drift detector we would like to point out that the achieved resolution of 18 μm x 24 μm in the detector of the active area of 17 mm x 11 mm corresponds to 4 x 10^5 resolution (precision) elements.

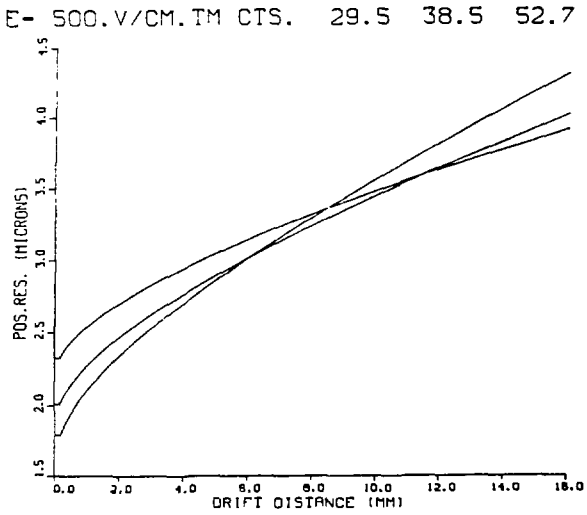

Fig. 9

This number of elements was achieved with 41 readout channels.

4. X-Ray Energy Measurement

A drift detector intended mainly for energy measurement is shown in Fig. 6 of Ref. [4]. Rectifying $p^+\nu$ junctions are concentric rings with a small, point-like anode at the center. The drift field has a cylindrical symmetry and electrons drift radially toward the anode. The active volume of the detector has a diameter of 1 cm and the anode capacitance is only 0.06pF.

A. Energy Resolution at Room Temperature

For the room temperature test the detector anode was connected to a charge sensitive preamplifier realized in hybrid technology on ceramic substrate from where the detector was mechanically supported. Special attention was paid to keep all stray input capacitancies at a minimum. Total input capacitance was 5pF from which 3pF was the gate capacitance of the first transistor of the preamplifier (2N4416).

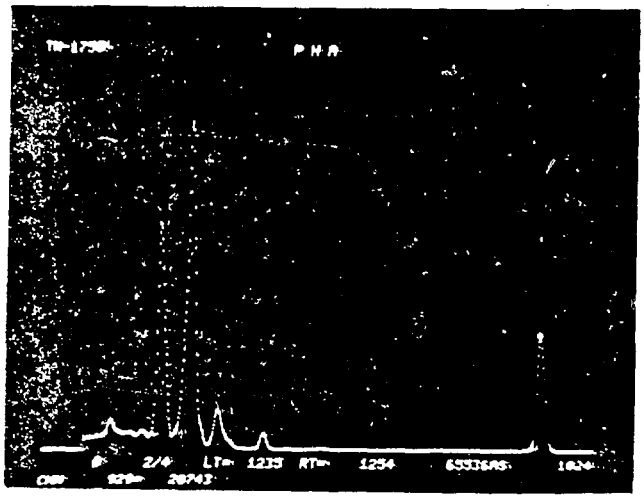

Fig. 10

Figures 10 and 11 show the spectrum of an Am^{241} source on linear and logarithmic scales, respectively. The equivalent noise charge is 110 electrons, corresponding to a FWHM of 930 eV of energy.

The leakage current was about 3nA. The shaping was pseudo-gaussian with the peaking time of 250 ns. The short shaping time makes the detector suitable for high rate applications.

The present improvement in the noise performance compared to the noise performance of 300 electrons reported in Ref. [4] is mainly due to the decrease of the input capacitance. However, the detector capacitance is still only one percent of the total input capacitance and further improvements are possible by using better matched input transistors.

We have experienced unforseen problems during the test of the cylindrical drift detector. The problem was the parasitic coupling of the positive

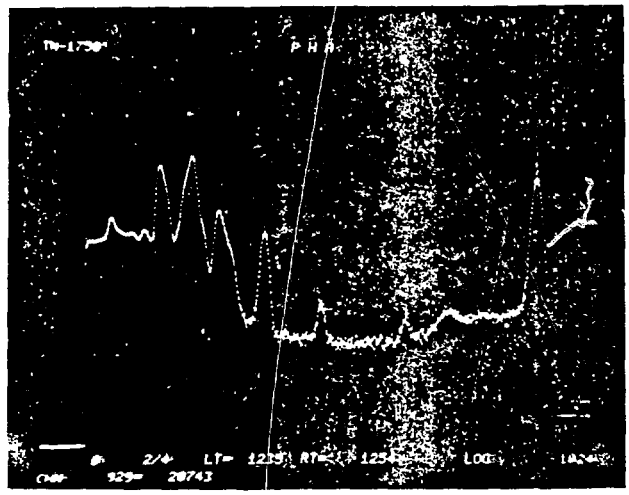

Fig. 11

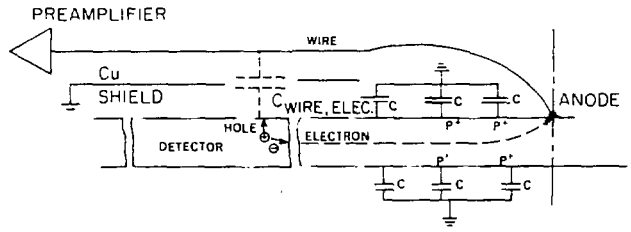

Fig. 12

charge of holes collected by rectifying $p^+\nu$ junctions to the input of the preamplifier. The mechanism of the coupling can be seen in Fig. 12 where the cylindrical detector is shown in the cross section together with a 25 μm diameter bonding wire which connects the anode to the preamplifier. The wire has its geometrical capacitance toward all ring shaped rectifying $p^+\nu$ junctions. If a junction which is not capacitively bypassed to ground receives holes produced by the ionization event, its potential changes due to the positive charge of holes. The change of the junction potential injects positive charge into the preamplifier through the above mentioned junction-wire capacitance (dotted capacitor in Fig. 12).

To eliminate this charge injection we have inserted a grounded Cu-shield between the detector and the wire. This solution might not be acceptable in certain applications of the detector. We are presently studying the feasibility of producing a cylindrical detector in which all junctions are bypassed with capacitors that are formed directly on the detector by photolithography (see below in discussion of self timing).

B. Energy Resolution at Liquid Nitrogen Temperature

The cylindrical detector was cooled down to liquid nitrogen temperature to test the electron transport properties and the energy resolution at low

temperature. The cryogenic and electronic system is a "conventional" system developed at Lawrence Berkeley Lab. [8] with the input field effect transistor operating close to the optimal temperature. The system has a physical 1000MΩ resistor in the feedback loop which limits its noise performance. The total input capacitance is again about 5pF, a mismatch factor of 100.

The equivalent noise charge with a pseudo-gaussian shaping of peaking time 3.2 μs was 36 electrons. This noise corresponds to an electronic energy resolution of 305 eV FWHM. The FWHM of Am^{241} 60 keV line (not shown) is 548 eV. The increase of the line width is consistent with a Fano factor of 0.17. This value should be interpreted only as an upper limit of Fano factor, because we are not sure if the Cu-shield was 100% effective in the low temperature geometry. We are now improving the geometry of the shield and we plan to use a system without a physical resistor in the feedback to improve the electronic noise and obtain a better measurement of the Fano factor.

The other important result is the absence of electron trapping in the material of the detector at liquid nitrogen temperature. We have compared positions of 60 keV Am^{241} peaks obtained at two different electrical potentials imposed on the detector.

i) Only a small volume of the detector close to the anode was active. Electrons traveled on average only .15 mm to reach the anode.

ii) The full volume of the drift detector was active. The mean distance traveled by electrons was about 4 mm.

We have not seen any shift in the peak position. From the statistics of these two measurements we estimate the electron trapping (0 ± 0.1)% for 4 mm drift length. This is equivalent to saying that the electron trapping time at liquid nitrogen temperature is longer than 100 μs.

C. Practical Biasing of Cylindrical Detectors

It is not practical to connect all ring shaped p^+v junctions of a cylindrical detector to an external voltage divider. It is possible to produce a voltage divider directly at the surface of the detector to alleviate the connection problem. (This solution was adopted for the multianode detector.) The drift field in the cylindrical detector is achieved automatically by biasing the last p^+v junction of the active detector volume to a sufficiently high negative potential. The drift field is a direct consequence of the existence of the maximum voltage between two neighboring rings (or strips) of rectifying p^+v junctions.

Figure 13, a close-up of Fig. 2, illustrates this existence. Fig. 13a shows the negative potential inside the detector close to the surface for a potential difference between two junctions less than the maximal difference shown in Fig. 13b. In Fig. 13a the negative potential decreases in all directions away from the junction for each point of the junction. (Heavily doped p^+ region of the junction is obviously at the same potential.) The decrease of the negative potential corresponds to a potential barrier for mobile holes in the p^+ region of the junction. The v-type silicon of the detector is depleted of electrons and there is practically no current flowing between two junctions.

If we continue to increase the negative potential applied on the first junction we arrive at

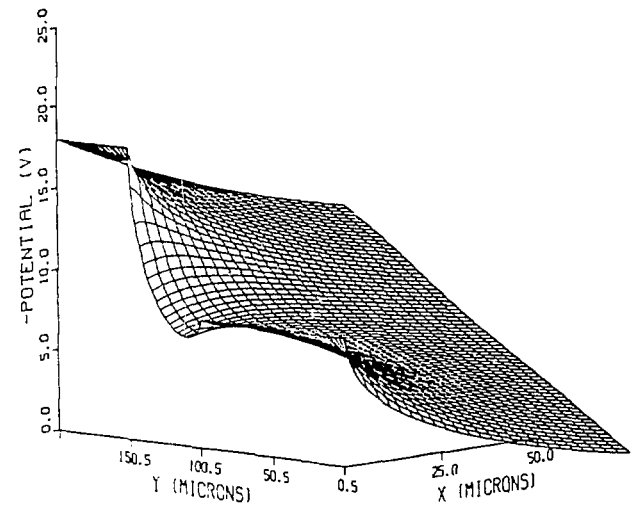

Fig. 13a

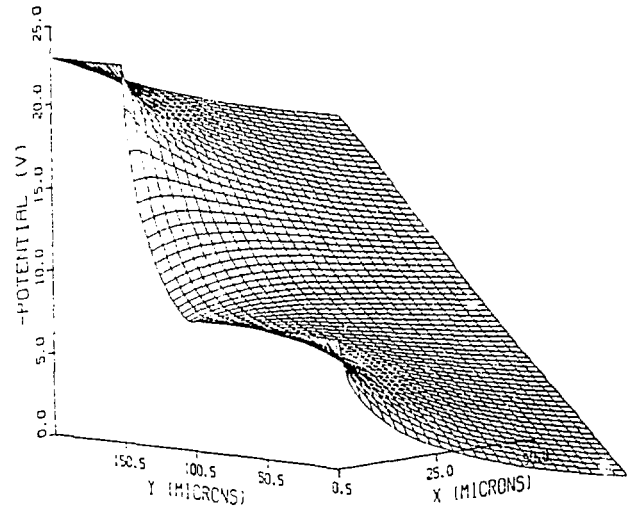

Fig. 13b

a potential configuration shown in Fig. 13b. At this value of the potential difference between two junctions the hole barrier of the second junction close to the first one has almost disappeared. If we increase further the negative potential on the first junction a disappearing hole barrier at the second junction allows mobile holes from the p region to escape. The charge taken away by escaping holes modifies the potential of the junction in such a way that the maximum difference is restored.

We have shown that the potential of the second junction follows the potential of the first one at the "distance" of the maximum potential difference. We also see that the third junction follows the second one etc. (chain effect), and the desirable potentials are established at all junctions of the detector drift region.

In actual operation the desirable voltage is imposed on the last junction of the chain and the

"high" voltage is imposed on the first junction through a large resistor (≈10-50MΩ). The correct voltages at all junctions are established when there is a certain amount of the hole chain current flowing from the last junction to the first one along the surface of the detector.

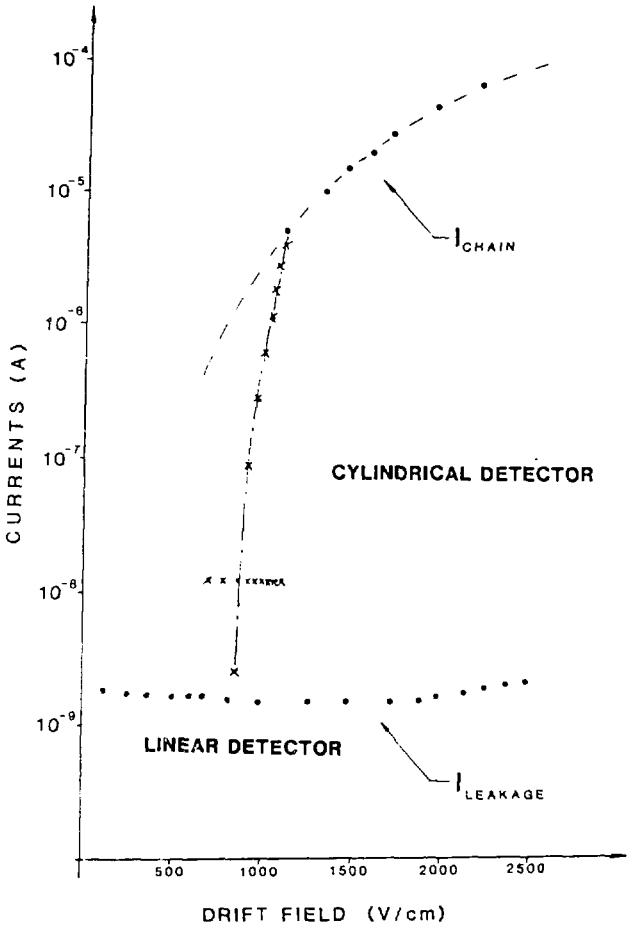

Fig. 14

Figure 14 shows the very strong dependence of the chain current on the average drift field for linear and cylindrical detectors. It also shows that the detector leakage current due to electrons flowing to the anode is independent of the chain (hole) current.

The advantage of the chain effect biasing is its simplicity. Its disadvantage is its dependence on the conditions of $Si-SiO_2$ interface and relatively narrow range of drift fields accessible with the chain biasing.

D. Self Timing of Drift Detectors

In our discussions of the position resolution in Section 3, we have been concerned with the detection of minimum ionizing particles. In the majority of experiments the time when the particle crosses the drift detector is known from other detectors used in the experiment (typically scintillators). To measure the position of a particle, the measurement of the arrival time of electrons at the anode is sufficient.

This is not the case in X-ray detection. In order to measure also the position in semiconductor drift detectors the time of X-ray conversion has to be measured by the detector itself.

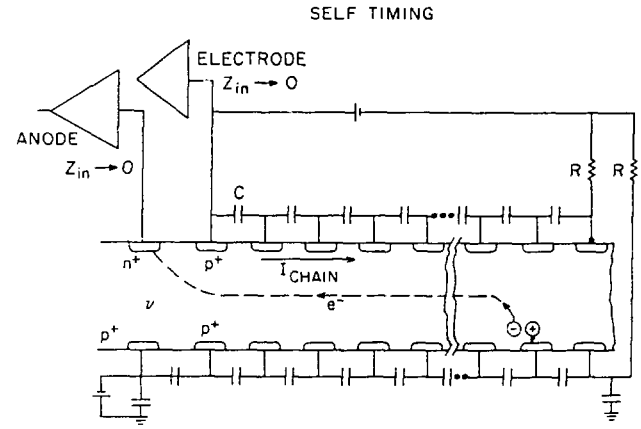

Fig. 15

The method is very similar to one used in Ref. [9]. Figure 15 shows capacitive connections of all rectifying $p^+\nu$ junctions together at both sides of the drift detector. One side is connected to the second preamplifier of the detector (called electrode amplifier at Fig. 15); the other side is bypassed to ground.

Electrons created by the conversion of an X-ray move toward the center plane of the detector while holes move to the closest surface of the detector. (We have assumed that the minimum of the potential energy of electrons is located in the center.) The movement of electrons and holes across the

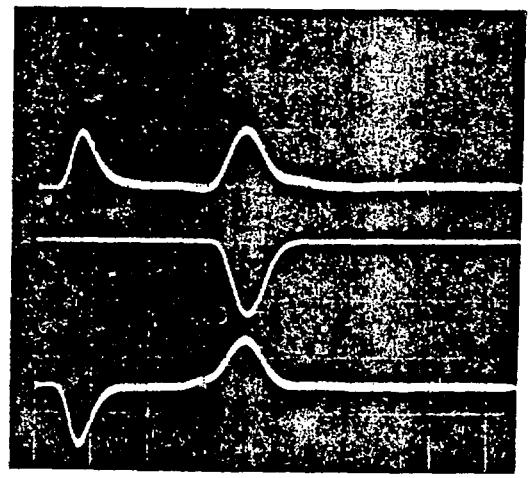

Fig. 16

detector induces a prompt signal in the preamplifier which defines the time of X-ray conversion.

Figure 16 displays output waveforms (time scale 200 ns/div.) of pseudo-gaussian shaping amplifiers which follow two preamplifiers of Fig. 15. The ionization effect of X-rays was simulated by a light pulser. The central trace shows the anode signal where only the delayed signal is present. The upper trace is the electrode signal when the light pulse shines on the top side of the detector, the lower trace is the electrode signal when the light pulse shines at the bottom side. All waveforms confirm our model of charge transport in semiconductor drift detectors.

We can see that the anode signal has less noise than the electrode signal which is a consequence of a significantly smaller anode capacitance compared to the electrode capacitance. Practically, an electrode signal measures the X-ray conversion time and an anode signal the electron arrival time and the X-ray energy.

The position resolution is not as good as in detection of minimum ionizing particles due to an additional timing error in the X-ray conversion measurement. For 60 keV X-rays the resolution is of order 100 μm, depending on the size of the detector.

Conclusions

Silicon drift detectors are reliable and versatile devices for position and energy measurement. They achieve the following performance parameters.

i) Position resolution for minimum ionizing particles
   a) σ = 4 μm under lab conditions
   b) σ = 11 μm in the beam test.
ii) Unambiguous two dimensional position resolution $\sigma \doteq$ 20 μm in the beam test.
iii) Energy resolution with equivalent noise charge
   a) ENC = 110 electrons at room temperature
   b) ENC = 36 electrons at liquid nitrogen temperature.
   The material of the detectors has a Fano factor smaller or equal to 0.17.
iv) Energy and position measurements are compatible.

We wish to thank V. Radeka for preamplifiers used in reported measurements, many stimulating discussions and, in particular, for the kind hospitality given to E. Gatti in the Instrumentation Division of BNL.

We are indebted to P. Solc for mounting and bonding of the detectors and to D. Stefani for modifying the preamplifier used for the energy measurement. D. Earley's careful preparation of the final script is acknowledged.

References

[1] E. Gatti and P. Rehak, Proc. 1983 DPF Workshop on Collider Detectors, Feb. 28-March 4, 1983, LBI-15973 UC-37, Conf. 830224, p. 97.

[2] E. Gatti and P. Rehak, Nucl. Instr. and Meth. 225, 608 (1984).

[3] E. Gatti, P. Rehak and J.T. Walton, Nucl. Instr. and Meth. 226, 129 (1984).

References (cont'd.):

[4] P. Rehak et al., Nucl. Instr. and Meth. A235, 224 (1985).

[5] E. Gatti et al., IEEE Trans. on Nucl. Sci., NS32, No. 2, 1204 (1985).

[6] P. Holl, Bau und Test einer Siliziumdriftkammer, Thesis, MPI München 1985.

[7] S.M. Sze, Physics of Semiconductor devices, Second Edition, John Wiley, New York 1981, p. 28.

[8] F.S. Goulding, J.T. Walton and D.F. Malone, Nucl. Instr. and Meth. 71, 273 (1969).

[9] P.N. Luke, N.W. Madden, F.S. Goulding, IEEE Trans. on Nucl. Sci. NS-32, 457 (1985).